Proceedings of the CAS–CERN Accelerator School: Beam Injection, Extraction and Transfer, Erice, Italy, 10-19 March 2017, edited by B. Holzer, CERN Yellow Reports: School Proceedings, Vol. 5/2018, CERN-2018-008-SP (CERN, Geneva, 2018)

Resonant Extraction

P. J. Bryant
Retired, CERN, Geneva, Switzerland

Abstract
Resonant extraction has its roots in the early cyclotrons where the emphasis was on increasing inter-turn separation. High energy physics (HEP) synchrotrons followed in the 1960s, but this time the emphasis was on extending the spill time. This lecture will concentrate on the 1/3rd integer resonance extraction for synchrotrons that is widely used in medical machines.

Keywords
Resonant extraction; slow extraction; Kobayashi Hamiltonian.

1 Historical note

Resonant extraction has its roots in the early cyclotrons. These machines used scattering from an internal target to obtain an external proton beam, but the consequent activation and loss of intensity were strong incentives for change. In 1951, James Tuck and Lee Teng (Chicago cyclotron) suggested a resonant scheme that increased the amplitude of radial oscillations sufficiently in a single turn to clear the mouth of a magnetic extraction septum. A quantitative analysis that confirmed the principle of what was then known as the 'Peeler-Regenerative Beam Extraction Method' was published by Kenneth Le Couteur (Liverpool cyclotron) in 1953 and the first successful extraction by this technique was demonstrated in the Liverpool cyclotron in 1954. This was reported by Albert Crewe and Le Couteur in 1955. At this stage, the emphasis was on increasing inter-turn separation.

High energy physics (HEP) synchrotrons in the 1950s were equipped with full-aperture, fast kickers for extraction. Single-turn extraction was efficient, but for fixed-target experiments it overloaded the physics counters leading to dead time and lost data. In 1961, Hugh Hereward addressed this problem [1] and his proposal cites Tuck, Teng, and Le Couteur. At essentially the same time, C. L. Hammer and Lawrence Jackson Laslett published a similar paper [2]. In contrast to cyclotrons, the emphasis was now on extending the spill time and a new name 'slow extraction' came into general usage.

2 Overview

For extraction, cyclotrons and synchro-cyclotrons work with the integer or half-integer resonance. This is consistent with a need for a large inter-turn separation and a fast extraction. To complete the historical picture, it is noted that in the 1980s, this situation changed for high-intensity proton cyclotrons with the introduction of H minus extraction[I].

In contrast, the extraction from synchrotrons works with the half-integer or 1/3rd integer resonance. The half-integer resonance is usually associated with fixed-target physics and spills of a few milliseconds while the 1/3rd integer resonance is weaker and is used widely in medical machines for spills of a few seconds (i.e., a few 10^6 turns). Higher-order resonances are not used because the resonances are weaker, the transit times in the resonances are longer, and the extraction separatrices

I The introduction of H minus extraction was something of a revolution that made the IBA Cyclone 30 a *de facto* world standard for isotope production.

https://doi.org/10.23730/CYRSP-2018-005.315

become too crowded making it difficult to ensure sufficient free aperture for the extraction equipment. Figure 1 shows some phase-space sketches to illustrate this last point. The present lecture will concentrate on the 1/3rd integer resonance.

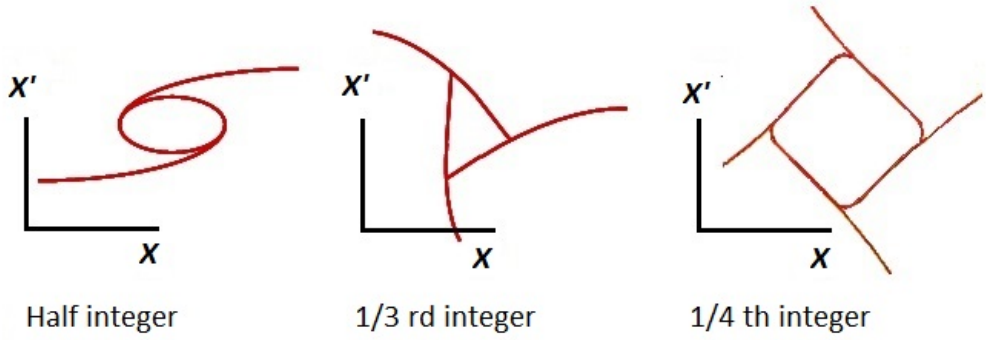

Fig. 1: Phase-space sketches of the half, 1/3rd, and 1/4th integer resonances

3 Phase space

The full beauty of resonant extraction is only visible in phase space. Figure 2 shows a 1/3rd integer extraction as designed for a medical machine. This diagram was generated by tracking single particles with progressively larger betatron amplitudes in the horizontal plane, but all with the same momentum (equivalent to the same horizontal position and tune). For the case shown, the relative momentum deviation with respect to the position of the resonance was about 0.001.

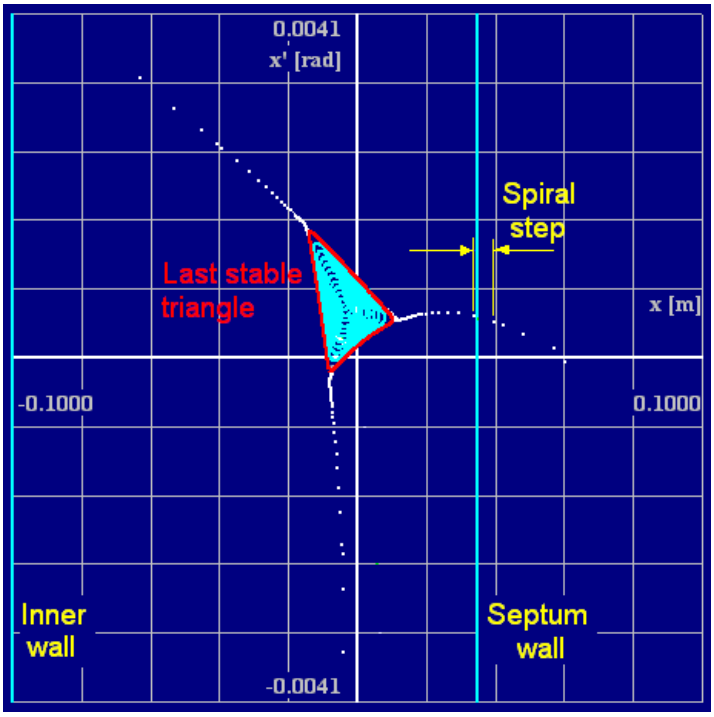

Fig. 2: Horizontal phase-space diagram of a 1/3rd integer extraction (annotated screen shot, WinAgile)

In the central region of Fig. 2, the beam has small betatron amplitudes and is stable. At the very centre, the invariants of the motion are unperturbed ellipses. At larger amplitudes, but still inside the

stable central region, the ellipses take on a triangular shape. In the outer region, the beam is unstable. The unstable part of the diagram is generated by one ion that 'locks' onto the 3 separatrices and gains amplitude turn after turn, while moving from one separatrix to the next.

The phase-space presentation has the advantage that the spiral step (inter-turn separation) and other geometric details can be determined to a high precision to facilitate the design of the extraction elements. By plotting this diagram for a range of momenta close to the resonance, it is possible to see how the 'last stable triangle' and the separatrices develop as a function of the tune separation from the resonance. In most cases, it is sufficient to consider just two limiting cases that define the beam, or the part of the beam that is being extracted. Before continuing to the quantitative analysis, it is useful to look at some other descriptive diagrams that describe slow extraction.

4 Other descriptive views of extraction

4.1 A 'strip' spill

The Steinbach diagram (attributed to C. Steinbach, CERN) has the advantages of being more holistic and showing the inclined threshold between stability and instability. The diagram plots the 'waiting' beam, the resonance and the spill using the radial position versus the effective, normalized amplitude of the betatron motion, $A_x = \sqrt{(E_x/\pi)}$, where E_x is the ion's motion invariant sometimes referred to as the single-particle emittance.

In the first example shown in Fig. 3, a wide momentum stack is being accelerated by a betatron core into the resonance. The tune of the resonance is usually close to the centre of the chamber and the chromaticity is finite and positive. Figure 2 corresponds to a snapshot of the phase space at an arbitrary point on the inclined stability boundary between the points 'A' and 'B' which define the part of the beam that is being extracted and correspond to the limiting cases referred to the last section. In this case, the phase-space snapshot would change significantly with position between 'A' and 'B'.

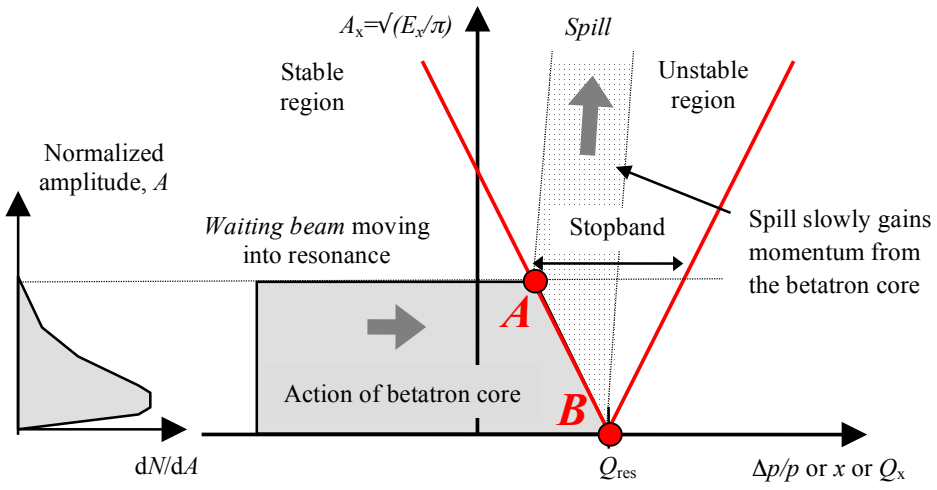

Fig. 3: An example of a Steinbach diagram for a momentum-driven slow extraction

In the second example shown in Fig. 4, a narrow momentum stack is being driven into the unstable region of the resonance by RF excitation at the revolution frequency causing amplitude growth. The limiting points denoted by 'A' and 'B' now define the top and bottom of the waiting beam and hence also the limits of the spill being extracted. As before, Fig. 4 corresponds to a snapshot of the phase space

somewhere between ‘A’ and ‘B’. In this case, the phase-space snapshot would be quasi-constant across the space from ‘A’ to ‘B’.

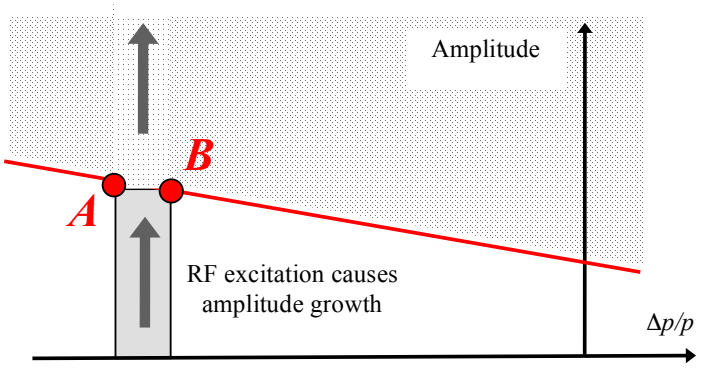

Fig. 4: Steinbach diagram of an amplitude-driven slow extraction

4.2 Near real-world view

The pictorial presentation in Fig. 5 is closer to the real-world situation of the momentum-driven extraction shown in Fig. 3. The waiting beam on the left is created by multi-turn injection in the inner half of the aperture well away from the 1/3rd integer resonance. After trapping and acceleration to the extraction energy, a betatron core is used to smoothly accelerate the waiting beam into the resonance, which is now positioned at the centre of the chamber. The particles ‘locked’ in the resonance grow in radial amplitude in steps of 3 turns. Starting with small steps, they extend outwards typically over several hundred turns before reaching the electrostatic extraction septum (ES). The beam enters the ES with a final step of ~10 mm and is kicked onto the extraction trajectory.

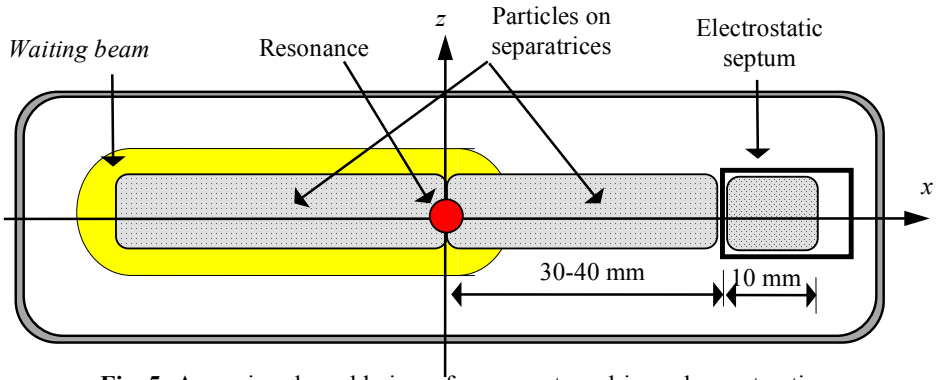

Fig. 5: A quasi-real-world view of a momentum-driven slow extraction

5 Sextupole fields

The radial 1/3rd integer or third-order resonance is driven by normal sextupole fields and can be treated as a perturbation to the linear machine. The transverse fields in a normal sextupole magnet are well known and can be written as,

$$B_x(x,z) = -6B_3xz \quad \text{and} \quad B_z(x,z) = -3B_3(x^2 - z^2)\ , \tag{1}$$

where

$$B_3 = -\frac{1}{6}\left(\frac{\mathrm{d}^2 B_z}{\mathrm{d}x^2}\right)_0 . \tag{2}$$

Thus, for a positively charged ion in an anticlockwise ring, the kicks given by a sextupole will be,

$$\Delta x' = \frac{B_z \ell_S}{|B\rho|} = \frac{1}{2}\frac{\ell_S}{|B\rho|}\left(\frac{\mathrm{d}^2 B_z}{\mathrm{d}x^2}\right)_0 \left(x^2 - z^2\right) = \frac{1}{2}\ell_S k'\left(x^2 - z^2\right), \tag{3}$$

$$\Delta z' = -\frac{\ell_S}{|B\rho|}\left(\frac{\mathrm{d}^2 B_z}{\mathrm{d}x^2}\right)_0 xz = -\ell_S k' xz \ , \tag{4}$$

where k' is the 'normalized sextupole gradient', $k' = \frac{1}{|B\rho|}\left(\frac{\mathrm{d}^2 B_z}{\mathrm{d}x^2}\right)_0$. (5)

6 Normalized coordinates

It is usual at this stage to introduce 'normalized coordinates'. Starting from the real-world position and angle of a test ion expressed with the usual Twiss parameters,

$$y(s) = C\beta^{1/2}(s)\cos\{\mu(s) + D\}, \tag{6}$$

$$y'(s) = -C\beta^{-1/2}(s)\left[\alpha(s)\cos\{\mu(s) + D\} + \sin\{\mu(s) + D\}\right], \tag{7}$$

where C and D are constants and y can be either of the transverse coordinates x or z. The phase terms can be isolated and used to define new coordinates $Y(\mu)$ and $Y'(\mu)$ that are known as normalized coordinates.

$$Y(\mu) = C\cos(\mu + D) = y(s)\beta^{-1/2} \tag{8}$$

$$Y'(\mu) = -C\sin(\mu + D) = y(s)\alpha\beta^{-1/2} + y'(s)\beta^{1/2} \ . \tag{9}$$

Note that the independent variable for real-world coordinates is s while for normalized coordinates it is μ. In line with general usage, normalized coordinates have upper case letters and real-world coordinates have lower case letters.

The object now is to express the motion of a test ion in normalized coordinates while crossing a sextupole. To simplify the analysis only a 'thin' sextupole (i.e., a sextupole with zero thickness) will be considered. This approximation is well justified in most cases. Under this assumption, the increments excited by the sextupole will be,

$$\Delta Y = 0, \quad \Delta y = 0 \quad \text{and} \quad \Delta Y' = \beta^{1/2}\,\Delta y'. \tag{10}$$

Assuming the *de facto* standard configuration of a horizontal ring and a normal sextupole, the kicks received in the horizontal and vertical planes are given by Eqs. (3) and (4) and substitution into Eq. (10) gives,

$$\Delta X' = \beta_x{}^{1/2}\Delta x' = \frac{1}{2}\beta_x{}^{1/2}\ell_S k'\left(x^2 - z^2\right)$$

$$\Delta Z' = \beta_z{}^{1/2}\Delta z' = -\beta_z{}^{1/2}\ell_S k' xz \ .$$

Using Eq. (8), these kicks become,

$$\Delta X' = \frac{1}{2}\beta_x{}^{3/2}\ell_S k'\left(X^2 - Z^2\frac{\beta_z}{\beta_x}\right)$$

$$\Delta Z' = -2\left(\frac{1}{2}\beta_x{}^{3/2}\ell_S k'\right)\frac{\beta_z}{\beta_x}XZ \ .$$

During the extraction process, the amplitude x increases to almost the full half-aperture, while z remains small. On this basis, the motion in z is neglected to first order and the final formulation of the sextupole kicks to be used for the extraction analysis is

Thin sextupole kicks:
$$\Delta X = \Delta Z = 0, \qquad \Delta X' = SX^2 \quad \text{and} \quad \Delta Z' = 0 \ . \tag{11}$$

where
$$S = \frac{1}{2}\beta_x{}^{3/2}\ell_S k' \ . \tag{12}$$

7 Basic theory of the resonance

The horizontal transfer matrix M_n for normalized coordinates, describing n turns in the machine is given by:

$$\boldsymbol{M}_n = \begin{pmatrix} \cos 2\pi(nQ_x) & \sin 2\pi(nQ_x) \\ -\sin 2\pi(nQ_x) & \cos 2\pi(nQ_x) \end{pmatrix} . \tag{13}$$

Consider an ion with a horizontal betatron tune close to a third-integer resonance, so that $Q_x = m \pm 1/3 + \delta Q$, where m is integer and $|\delta Q| << 1/3$). The tune increment δQ is defined as the tune distance of the ion from the resonance,

$$\delta Q = Q_{\text{particle}} - Q_{\text{resonance}} \ . \tag{14}$$

The explicit transfer matrix for n turns in the unperturbed machine can then be written as

$$\boldsymbol{M}_n = \begin{pmatrix} \cos\left[2n\pi\left(m \pm 1/3 + \delta Q\right)\right] & \sin\left[2n\pi\left(m \pm 1/3 + \delta Q\right)\right] \\ -\sin\left[2n\pi\left(m \pm 1/3 + \delta Q\right)\right] & \cos\left[2n\pi\left(m \pm 1/3 + \delta Q\right)\right] \end{pmatrix} . \tag{15}$$

Thus, to a good approximation the coordinates of the ion after one, two and three turns become:

1st turn neglecting δQ:
$$\begin{pmatrix} X \\ X' \end{pmatrix}_1 \cong \begin{pmatrix} -1/2 & \pm\sqrt{3}/2 \\ \mp\sqrt{3}/2 & -1/2 \end{pmatrix}\begin{pmatrix} X \\ X' \end{pmatrix}_0 \tag{16}$$

2nd turn neglecting δQ:
$$\begin{pmatrix} X \\ X' \end{pmatrix}_2 \cong \begin{pmatrix} -1/2 & \mp\sqrt{3}/2 \\ \pm\sqrt{3}/2 & -1/2 \end{pmatrix}\begin{pmatrix} X \\ X' \end{pmatrix}_0 \tag{17}$$

3rd turn with δQ:
$$\begin{pmatrix} X \\ X' \end{pmatrix}_3 \cong \begin{pmatrix} 1 & \varepsilon \\ -\varepsilon & 1 \end{pmatrix}\begin{pmatrix} X \\ X' \end{pmatrix}_0 \ , \tag{18}$$

where ε replaces $6\pi\delta Q$ for brevity . The small quantity ε is called the 'modified tune distance'. It can be seen that an ion with exactly the resonant tune (i.e., $\varepsilon = 0$) will return to its initial position every three turns.

The effect of the sextupole during three turns in the machine is now calculated as a perturbation by the linear addition of 3 instances using Eqs. (16), (17), and (18):

(A) The effect of 3 turns with a sextupole placed after the 3rd turn,
M3 + Sextupole;

(B) The effect of 3 turns with a sextupole placed after the 2nd turn,
M2 + Sextupole + M1;

(C) The effect of 3 turns with a sextupole placed after the 1st turn
M1 + Sextupole + M2.

In (A), (B), and (C), the sextupole is represented by the simplified, thin-lens kicks from Eqs. (11) and (12). Filling out the steps (A), (B), and (C) explicitly yields:

$$\text{(A)}\quad \left\{\begin{aligned} X_3 &= \left(X_0 + \varepsilon X_0'\right) \\ X_3' &= -\varepsilon X_0 + X_0' + S\left(X_0 + \varepsilon X'\right)^2 \end{aligned}\right\}.$$

$$\text{(B)}\quad \left\{\begin{aligned} X_3 &= -\frac{1}{2}\left(-\frac{1}{2}X_0 \mp \frac{\sqrt{3}}{2}X'\right) \pm \frac{\sqrt{3}}{2}\left[\pm\frac{\sqrt{3}}{2}X_0 - \frac{1}{2}X_0' + S\left(-\frac{1}{2}X_0 \mp \frac{\sqrt{3}}{2}X_0'\right)^2\right] \\ X_3' &= \mp\frac{\sqrt{3}}{2}\left(-\frac{1}{2}X_0 \mp \frac{\sqrt{3}}{2}X'\right) - \frac{1}{2}\left[\pm\frac{\sqrt{3}}{2}X_0 - \frac{1}{2}X_0' + S\left(-\frac{1}{2}X_0 \mp \frac{\sqrt{3}}{2}X_0'\right)^2\right] \end{aligned}\right\}.$$

$$\text{(C)}\quad \left\{\begin{aligned} X_3 &= -\frac{1}{2}\left(-\frac{1}{2}X_0 \pm \frac{\sqrt{3}}{2}X'\right) \mp \frac{\sqrt{3}}{2}\left[\mp\frac{\sqrt{3}}{2}X_0 - \frac{1}{2}X_0' + S\left(-\frac{1}{2}X_0 \pm \frac{\sqrt{3}}{2}X_0'\right)^2\right] \\ X_3' &= \pm\frac{\sqrt{3}}{2}\left(-\frac{1}{2}X_0 \pm \frac{\sqrt{3}}{2}X'\right) - \frac{1}{2}\left[\mp\frac{\sqrt{3}}{2}X_0 - \frac{1}{2}X_0' + S\left(-\frac{1}{2}X_0 \pm \frac{\sqrt{3}}{2}X_0'\right)^2\right] \end{aligned}\right\}.$$

After the addition of the three steps (A), (B), and (C) shown above, only first-order correction terms in ε are retained to give:

$$\Delta X_3 = \varepsilon X_0' \pm \frac{\sqrt{3}}{2}S\left(-\frac{1}{2}X_0 \mp \frac{\sqrt{3}}{2}X_0'\right)^2 \mp \frac{\sqrt{3}}{2}S\left(-\frac{1}{2}X_0 \pm \frac{\sqrt{3}}{2}X_0'\right)^2$$

$$\Delta X_3' = -\varepsilon X_0 + SX_0^2 - \frac{1}{2}S\left(-\frac{1}{2}X_0 \mp \frac{\sqrt{3}}{2}X_0'\right)^2 - \frac{1}{2}S\left(-\frac{1}{2}X_0 \pm \frac{\sqrt{3}}{2}X_0'\right)^2.$$

The cancellation of signs shows that there is no fundamental difference between the 1/3rd and 2/3rd resonances.

$$\Delta X_3 = \varepsilon X_0' + \frac{\sqrt{3}}{2} S\left(-\frac{1}{2}X_0 - \frac{\sqrt{3}}{2}X_0'\right)^2 - \frac{\sqrt{3}}{2} S\left(-\frac{1}{2}X_0 + \frac{\sqrt{3}}{2}X_0'\right)^2$$

$$\Delta X_3' = -\varepsilon X_0 + SX_0^2 - \frac{1}{2}S\left(-\frac{1}{2}X_0 - \frac{\sqrt{3}}{2}X_0'\right)^2 + \frac{1}{2}S\left(-\frac{1}{2}X_0 + \frac{\sqrt{3}}{2}X_0'\right)^2 .$$

Finally, the expressions for the changes in position and divergence of the ion, known as the 'spiral step' and 'spiral kick', over three revolutions, are obtained as:

Spiral step:
$$\Delta X_3 = \varepsilon X_0' + \frac{3}{2} S X_0 X_0' . \tag{19}$$

Spiral kick:
$$\Delta X_3' = -\varepsilon X_0 + \frac{3}{4} S\left(X_0{}^2 - X_0'^2\right) \tag{20}$$

8 Kobayashi Hamiltonian

The time needed for three revolutions in the machine is short compared to the spill time and can be safely used as the basic unit of time. The elementary changes occurring in this unit of time are the smallest that need to be resolved to understand the physics of the extraction. Thus the subscripts in Eqs. (19) and (20) are no longer needed and the kicks can be treated as a continuous function that is derived from a Hamiltonian $\boldsymbol{H}$, such that

$$\Delta X_3 \Rightarrow \left(\frac{\Delta X}{\Delta t}\right)_{\Delta t = 1\,(3\text{ turn})} = \frac{\partial \boldsymbol{H}}{\partial X'} = \varepsilon X' + \frac{3}{2} S X X' \ , \tag{21}$$

$$\Delta X'_3 \Rightarrow \left(\frac{\Delta X'}{\Delta t}\right)_{\Delta t = 1\,(3\text{ turn})} = -\frac{\partial \boldsymbol{H}}{\partial X} = -\varepsilon X + \frac{3}{4} S\left(X^2 - X'^2\right) . \tag{22}$$

The Kobayashi Hamiltonian [3,4] is found by integrating the above partial differentials Eqs. (21) and (22). It should be noted that in this formulation time is dimensionless.

Kobayashi Hamiltonian:
$$\boldsymbol{H} = \frac{\varepsilon}{2}\left(X^2 + X'^2\right) + \frac{S}{4}\left(3XX'^2 - X^3\right) . \tag{23}$$

The Hamiltonian is time independent and a constant of the motion. Contours of constant $\boldsymbol{H}$ show the particle trajectories in normalized phase space at the sextupole. This presentation of the motion is known as a 'phase-space map'. The first term in Eq. (23) describes the unperturbed particle motion in the linear, machine (i.e., $S = 0$). These trajectories are circles of radius $\sqrt{(2\boldsymbol{H}/\varepsilon)}$ in normalized phase space. The second term contains the perturbation that distorts the circular phase-space trajectories into a triangular form as illustrated in Figs. 2 and 6. At a certain level of excitation, the triangle 'breaks' into open phase-space trajectories forming the three separatrices. A change in sign of either the modified tune distance ε or the normalized sextupole strength S is equivalent to a rotation of the phase-space trajectories by 180º.

All the properties of the system can be derived from the Hamiltonian. In particular, when $\boldsymbol{H}$ has the value $[(2\varepsilon/3)^3/S^2]$, it factorizes into three straight lines

$$\left(\frac{S}{4}X + \frac{\varepsilon}{6}\right)\left(\sqrt{3}X' + X - \frac{4\varepsilon}{3S}\right)\left(\sqrt{3}X' - X + \frac{4\varepsilon}{3S}\right) = 0 \ , \tag{24}$$

called the 'separatrices' that define the boundaries between the 'last stable triangle' and unstable regions in phase space. The phase-space area of the stable region is the 'acceptance' of the system at the given momentum. It could also be regarded as the 'dynamic aperture'. The size of the stable region is determined by the ratio $|\varepsilon/S|$. For an ion that has exactly the resonant tune the stable region shrinks to zero.

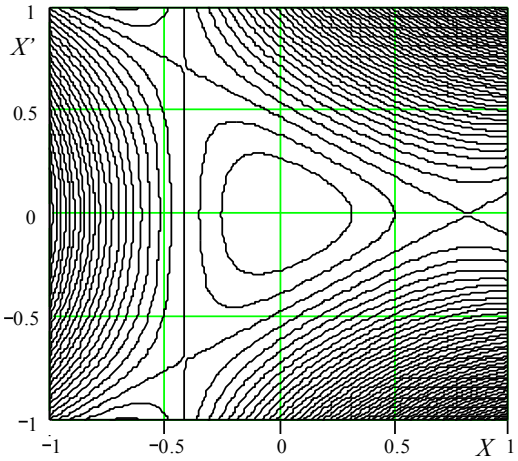

Fig. 6: Phase-space map at the resonance sextupole (plotted from the Kobayashi Hamiltonian)

Figure 7 defines the geometry of the separatrices at the sextupole and the four stable fixed points, P_0 to P_3.

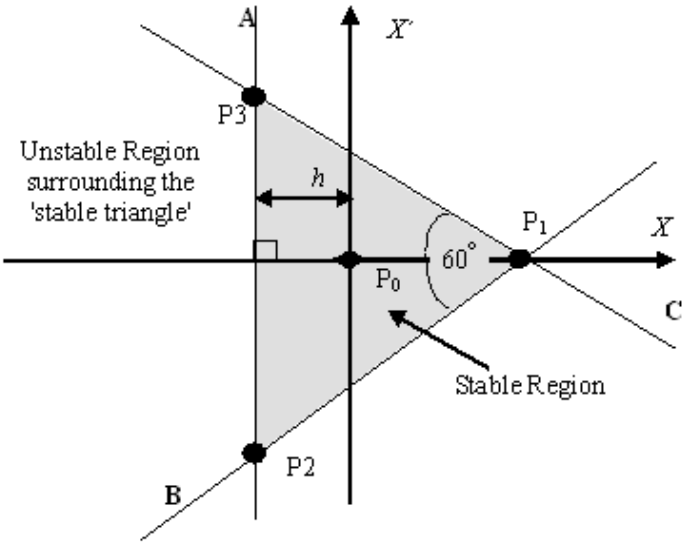

$$P_1 = \left(\frac{4}{3}\frac{\varepsilon}{S}, 0\right)$$

$$P_2 = \left(-\frac{2}{3}\frac{\varepsilon}{S}, -\frac{2\varepsilon}{\sqrt{3}S}\right)$$

$$P_3 = \left(-\frac{2}{3}\frac{\varepsilon}{S}, \frac{2\varepsilon}{\sqrt{3}S}\right)$$

$$h = \frac{2}{3}\frac{\varepsilon}{S} = \frac{4\pi}{S}\delta Q$$

Fig. 7: Geometry of the phase-space map at the resonance-excitation sextupole

The geometry of the last stable triangle is conveniently described by introducing the distance h between the upright separatrix A and the X'-axis. A change in the sign of h is equivalent to a 180° rotation of the stable triangle around the origin.

$$h = \frac{2}{3}\frac{\varepsilon}{S} = \frac{4\pi}{S}\delta Q \,. \tag{25}$$

The area (i.e., the acceptance) of the last stable triangle can also be expressed in terms of h as,

Acceptance of last stable triangle: $$\text{Area} = 3\sqrt{3}h^2 = \frac{48\sqrt{3}\pi}{S^2}(\delta Q)^2\pi \ . \tag{26}$$

Providing the sextupole is powered in an adiabatic way, the emittance will be conserved and Eq. (26) gives the fraction of the original beam emittance that remains stable.

Since Figs. 6 and 7 are in normalized phase space, the unperturbed trajectories are circles and X is equivalent to X'. Hence, we can rotate the diagram to any position around the machine using the betatron phase to determine the position without altering its shape.

9 Comment on resonances

If this were a lecture on resonances, a more advanced Hamiltonian would be used in order to describe the general case of mixed horizontal and vertical resonances driven by normal and skew fields over much larger apertures. Some examples showing the variety of patterns generated by the relatively simple half-integer resonances are illustrated in Fig. 8.

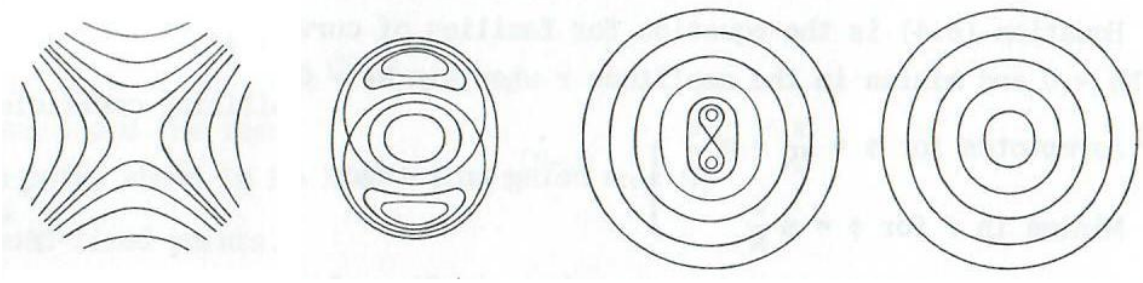

Fig. 8: Examples of the various phase-space views excited by the half-integer resonance

In this lecture, a simplified Hamiltonian has been used. This is justified since only a purely radial 1/3$^{\text{rd}}$ integer resonance is being considered and, furthermore, the trajectories are being intercepted within the physical aperture of the machine before more exotic features such as distant stable islands can be formed. It is stressed, that this is a simplified situation that is only used to obtain basic parameters such as the spiral step and to provide some insight into how the slow extraction works. In practice, it is essential to back up these estimations with numerical calculations using a lattice program.

10 The virtual sextupole

In most rings, sextupoles are mounted in dispersion regions for controlling the chromaticity and they are positioned so as to cause as little resonance excitation as possible, but their mutual compensation is never perfect. For slow extraction, a dedicated sextupole for exciting the resonance will be needed and this sextupole is best positioned in a zero-dispersion region, so as not to disturb the chromaticity correction. The dedicated resonance sextupole, which will be dominant, the residual excitation from the chromaticity sextupoles and any sextupole errors from the machine (mainly from the dipoles) can be combined numerically into a single virtual sextupole. This virtual sextupole will behave according to the theory presented so far.

For the 1/3$^{\text{rd}}$ integer resonance $3Q_{\text{x}} = p$, the driving term is found by integrating the normal sextupole components around the whole ring according to [5],

$$\kappa(s_0) = \frac{1}{24\sqrt{\pi C}} \int_{s_0}^{s_0+C} \beta_x^{3/2} \left[\frac{-1}{|B_0\rho|} \left(\frac{\mathrm{d}^2 B_z}{\mathrm{d}x^2} \right)_0 \right] \exp(3\mathrm{i}\mu_x)\mathrm{d}s \ , \tag{27}$$

using the earlier definition for S in Eq. (12) and assuming short elements gives,

$$\kappa(s_0) = \frac{-1}{12\sqrt{\pi C}} \sum_{\mathrm{n}} S_{\mathrm{n}} \exp\left(3\mathrm{i}\mu_{\mathrm{x,n}}\right). \tag{28}$$

The virtual sextupole can be found by equating its driving term to the sum of all the driving terms around the ring as given by Eq. (28) and separating the real and imaginary parts to give,

$$S_{\mathrm{virt}} \cos\left(3\mu_{\mathrm{x,virt}}\right) = \sum_{\mathrm{n}} S_{\mathrm{n}} \cos\left(3\mu_{\mathrm{x,n}}\right), \tag{29}$$

$$S_{\mathrm{virt}} \sin\left(3\mu_{\mathrm{x,virt}}\right) = \sum_{\mathrm{n}} S_{\mathrm{n}} \sin\left(3\mu_{\mathrm{x,n}}\right). \tag{30}$$

Using Eqs. (29) and (30), the betatron phase (and hence the position) and the strength of the virtual sextupole can be found as

Virtual sextupole phase:

$$\tan\left(3\mu_{\mathrm{x,virt}}\right) = \frac{\sum_{\mathrm{n}} S_{\mathrm{n}} \sin\left(3\mu_{\mathrm{x,n}}\right)}{\sum_{n} S_{\mathrm{n}} \cos\left(3\mu_{\mathrm{x,n}}\right)}. \tag{31}$$

Virtual sextupole strength:

$$S_{\mathrm{virt}}^2 = \left[\sum_{\mathrm{n}} S_{\mathrm{n}} \cos\left(3\mu_{\mathrm{x,n}}\right)\right]^2 + \left[\sum_{\mathrm{n}} S_{\mathrm{n}} \sin\left(3\mu_{\mathrm{x,n}}\right)\right]^2. \tag{32}$$

11 Configuring the extraction

The basic theory in the earlier sections can be exploited in a number of practical configurations. These are listed briefly below with some comments on their use:

11.1 Moving the beam

This method has the advantage of leaving the transverse optical parameters of the machine constant, and hence also those of the resonance. There are two possibilities:

11.1.1 Momentum-driven

In this scenario the beam is accelerated towards the stationary resonance by a betatron core, or by stochastic noise, or possibly by phase displacement acceleration or a RF micro-bucket acceleration system. The principal requirement is to accelerate the beam smoothly and in a controlled way over say one to two seconds. The betatron core having a large inductance smooths out ripple and the steps made by the digital to analogue converter (DAC), but for the same underlying reason it is not ultra-fast to respond. Stochastic noise can be particularly slow acting and this method has been used for ultra-slow extractions lasting 30 minutes or more.

11.1.2 Amplitude-driven

In this case, the beam is excited by transverse stochastic noise or RF excitation at the revolution frequency, so that its betatron amplitudes grow. The chromaticity is set to near zero, so that the resonance line acts as a threshold in amplitude above which the ions become unstable. RF excitation of the

amplitude works well in the range of one to a few seconds and it is quick to respond when switched off [6].

11.2 Moving the resonance

This method is not recommended as it alters the transverse optics of the machine during the extraction. Because the optics is changing, on-line compensation systems are needed to keep the extracted beam at a constant position, angle, momentum spread, and intensity.

11.2.1 Quadrupole-driven

This is probably the first method ever used. The tune of the machine is changed by a quadrupole so as to move the resonance across the beam. In addition to the objections in section 11.2, this method is particularly sensitive to ripple in the power converter driving the extraction quadrupole.

11.2.2 Sextupole-driven

The resonance excitation is changed by increasing the strength of the resonance sextupole. This method is included only for academic completeness.

11.3 Equipment configuration

The momentum-driven and the amplitude-driven are the two most important configurations, but for brevity, this paper will focus on the momentum-driven extraction with all the extraction equipment in the positive, outer half of the aperture. There are of course other possibilities, but in general the principles remain unchanged. Placing the ES in the 1st quadrant requires the virtual sextupole to be positioned so that the chosen extraction separatrix advances around the machine to the ES where it has the angle of 45º±15º with respect to the *x*-axis. At this point, the ES intercepts the beam segment corresponding to the last three turns. This segment will be typically 10 mm in radial length. The ES wall, which is made of thin wires usually of 0.1 mm diameter will intercept an equivalent amount of beam (~1%). The beam segment inside the ES is given a radial kick typically of a few milliradians. Once this is done, the beams continue to the magnetic septum (MS). So as to maximize the gap between the end of the extraction separatrix and the segment of extracted beam, there is ideally a horizontal betatron phase advance of about 90º between the ES and MS to convert the kick to a physical gap at the MS of typically 20 mm. Figure 9 summarizes these points.

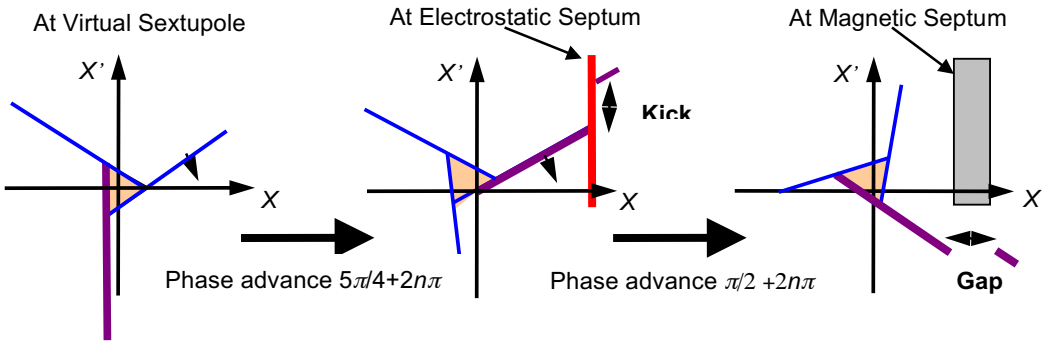

Fig. 9: Configuring the ES and MS for a slow extraction scheme

Of course, the ES and MS must also coincide with available drift spaces in the lattice and have suitable Twiss parameters. There are also further conditions to be considered such as the Hardt condition (see sections 12−14). The final configuration will inevitably be a series of compromises.

12 A more generalized Hamiltonian

The previous section referred to the Hardt condition, which is an important feature in slow extraction schemes. To derive this condition, it is necessary to extend the simple Kobayashi Hamiltonian given earlier to include the dispersion function [7]. To first order in momentum, the equilibrium orbit in normalized coordinates is given by:

$$X_{\mathrm{EQ.O}} = D_n \frac{\delta p}{p}, \quad X'_{\mathrm{EQ.O}} = D'_n \frac{\delta p}{p}\ , \tag{33}$$

where $(D_\mathrm{n}, D'_\mathrm{n})$ is the normalized dispersion vector and $\delta p/p$ is the fractional momentum deviation. A second coordinate system (X_β, X'_β) is introduced with its origin on the off-momentum equilibrium orbit. The particle coordinates are then split into a constant term, given by the dispersion function and a betatron term as shown in Fig. 10.

$$X = X_\beta + D_\mathrm{n} \frac{\delta p}{p} \quad \Leftrightarrow \quad X_\beta = X - D_\mathrm{n} \frac{\delta p}{p} \tag{34}$$

$$X' = X'_\beta + D'_\mathrm{n} \frac{\delta p}{p} \quad \Leftrightarrow \quad X'_\beta = X' - D'_\mathrm{n} \frac{\delta p}{p}\ . \tag{35}$$

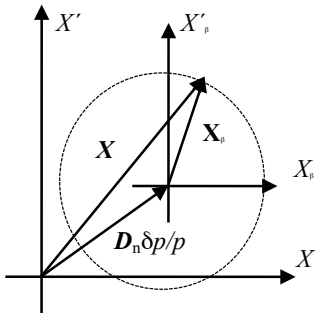

Fig. 10: Coordinates of the betatron motion

The general Hamiltonian is derived following the same steps as for the Kobayashi Hamiltonian except that the betatron motion and the total motion now have to be separated. The analysis starts with the betatron motion Eqs. (34) and (35) for n turns in the unperturbed machine, as before,

$$\begin{pmatrix} X_\beta \\ X'_\beta \end{pmatrix}_\mathrm{k} = \boldsymbol{M}_\mathrm{n} \begin{pmatrix} X_\beta \\ X'_\beta \end{pmatrix}_0\ . \tag{36}$$

The main difference appears when calculating the kick of the sextupole that now depends on the total motion of the ion,

Dispersion region: $$\Delta X_\beta = 0, \quad \Delta X'_\beta = SX^2 = S\left(X_\beta + D_n \frac{\delta p}{p} \right)^2\ . \tag{37}$$

This yields a more general Hamiltonian in the betatron coordinates (X_β, X'_β):

$$\boldsymbol{H} = \frac{\varepsilon}{2}\left(X_\beta^2 + X_\beta'^2\right) + \frac{S}{4}\left(3X_\beta X_\beta'^2 - X_\beta^3\right) - \frac{3}{2} S\left(D_\mathrm{n} \frac{\delta p}{p} \right)\left(X_\beta^2 + X_\beta'^2\right). \tag{38}$$

Re-ordering the terms in Eq. (38) shows that the dispersion-dependent term affects only the 'circular' trajectories and this can be considered as a change in the tune distance, ε.

General form: $$\boldsymbol{H} = \frac{1}{2}\left[\varepsilon - 3S\left(D_{\mathrm{n}}\frac{\delta p}{p}\right)\right]\left(X_\beta^2 + X_\beta'^2\right) + \frac{S}{4}\left(3X_\beta X_\beta'^2 - X_\beta^3\right). \tag{39}$$

Let $\delta\widetilde{Q}$ be the change in tune implied by the dispersion-dependent term in Eq. (39), so that

. $$\delta\widetilde{Q}_x = -\frac{1}{6\pi}3S\left(D_{\mathrm{n}}\frac{\delta p}{p}\right) = -\frac{1}{4\pi}\beta_{\mathrm{x}}\ell_{\mathrm{S}}k'D_{\mathrm{x}}\frac{\delta p}{p}. \tag{40}$$

By introducing the chromaticity $Q'_{\mathrm{x}} = \left(\frac{dQ_{\mathrm{x}}}{dp/p}\right)$ as the linear change of the betatron tune with momentum, the chromatic effect of the sextupole can be expressed as

$$Q'_{\mathrm{x}} = \left(\frac{d\widetilde{Q}_{\mathrm{x}}}{dp/p}\right) = -\frac{1}{4\pi}\beta\ell_{\mathrm{S}}k'D_{\mathrm{x}}, \tag{41}$$

which corresponds exactly to the classic linear form for the tune shift introduced by a sextupole.

The general Hamiltonian in Eq. (39) correctly describes the physics of a third-integer resonance to first order in a perfect lattice without any further restrictions on sextupole locations or particle momenta. The phase space at the sextupole has the same qualitative shape as the earlier simple theory, but it is scaled by the tune shift introduced by the sextupole. In readiness for the next topic, the geometry and general equations of the separatrices are given in Fig. 11. From these results, it is clear that any change in the sextupole strength will also change the tune distance of the particles and therefore the scale of the extraction phase space. This a second reason for putting the resonance sextupole in a dispersion-free region (the first reason was not to affect the chromaticity).

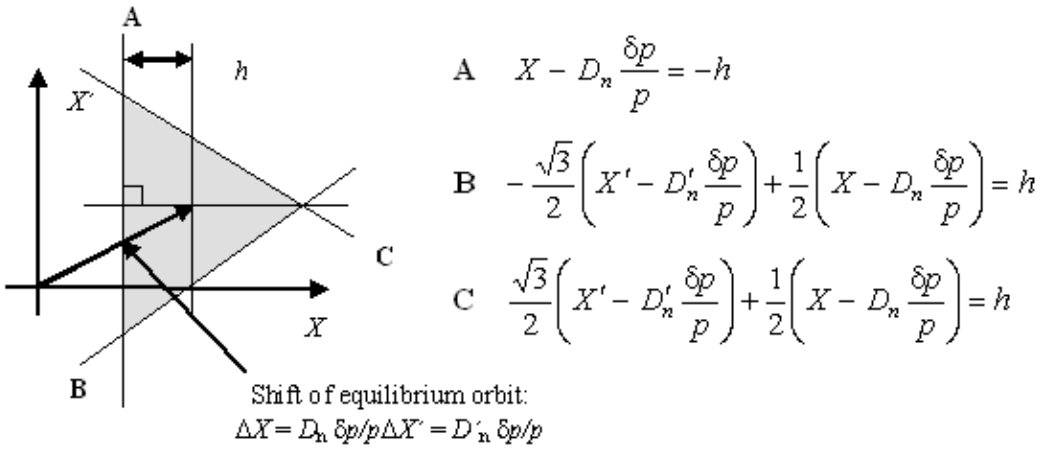

Fig. 11: Geometry of the separatrices at the sextupole for an off-momentum beam

The above can be further extended in an exactly analogous way for the effect of closed-orbit errors. This can be used to put limits on the closed-orbit variation that can be tolerated at the resonant sextupole.

13 Equations for separatrices

A general equation for a separatrix in the phase-space map can be constructed from the standard form for a straight line that uses the perpendicular distance (in this case *h*) from the origin Eq. (42) and Fig. 12.

Standard form: . (42)

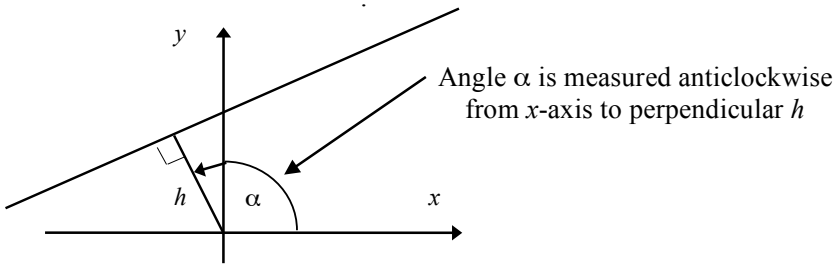

Fig. 12: Perpendicular form for a straight line

Combining Eq. (42) with the shift of origin corresponding to the dispersion vector yields the general equation for a separatrix.

$$\left(X - D_n(s)\frac{\delta p}{p}\right)\cos\alpha + \left(X' - D_n'(s)\frac{\delta p}{p}\right)\sin\alpha = h \ . \tag{43}$$

The separatrices rotate clockwise with the betatron phase advance $\Delta\mu$ measured from the sextupole. At any given position $\alpha = (\alpha_0 - \Delta\mu)$ and by inspection of Figs. 11 and 12 the values for α_0 at the sextupole are:

(A) $\alpha_0 = 180°$ (anticlockwise);

(B) $\alpha_0 = 300°$ (anticlockwise);

(C) $\alpha_0 = 420°$ (anticlockwise);

so that the three separatrices can be drawn at any position using,

$$\left(X - D_n(s)\frac{\delta p}{p}\right)\cos(\alpha_0 - \Delta\mu) + \left(X' - D_n'(s)\frac{\delta p}{p}\right)\sin(\alpha_0 - \Delta\mu) = h \ . \tag{44}$$

14 Hardt condition

Referring back to Fig. 3, it can be seen that in a momentum-driven extraction all ions on the line AB become unstable at the same time. Each point between A and B has its own momentum, its own stability threshold, its own transit time in the resonance and its own last stable triangle. This spread in parameters can be useful for smoothing ripple, but unless the extraction separatrices are all aligned there will be significant particle losses on the ES. Figure 13 illustrates the general case in real space. The last stable triangles are spread out and when the extraction separatrices reach the ES they all have different angles. Since the ES can only be aligned for one angle, losses will occur.

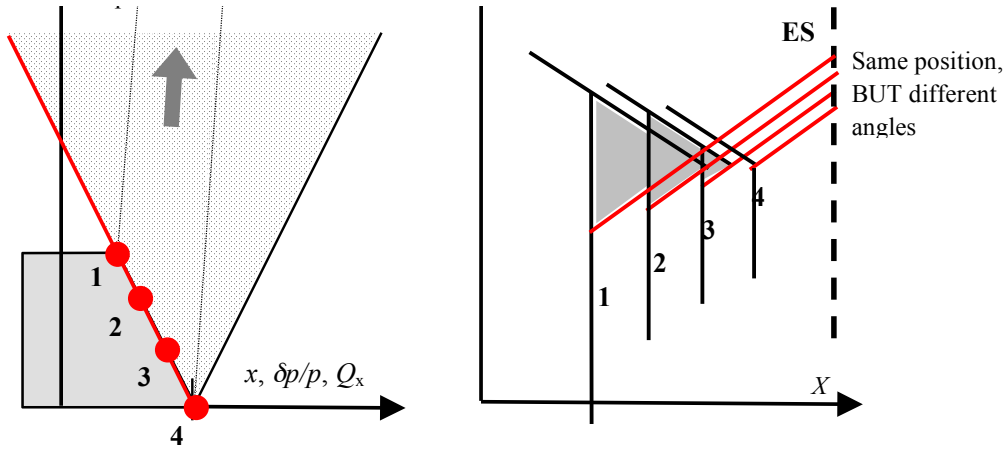

Fig. 13: A momentum-driven extraction without alignment of the separatrices

Minimum losses would be obtained if all the separatrices could be super-positioned. This is achieved by the Hardt condition [8]. Since the stable triangles have different momenta they are affected by the dispersion at the ES and by a suitable choice of the dispersion vector all the separatrices of the different momenta can be made to enter the ES with the same angle. The restrictions on the lattice functions to satisfy the Hardt condition can be derived with a purely mathematical approach from the general expression for the separatrix already given in Eq. (44). First Eq. (25) is rewritten using the chromaticity as,

$$h = \frac{2}{3}\frac{\varepsilon}{S} = \frac{4\pi}{S}\delta Q = \frac{4\pi}{S}Q'\frac{\delta p}{p} \,. \tag{45}$$

The substitution of Eq. (45) into Eq. (44) gives the general expression for a separatrix as a function of particle momentum and the chromaticity of the machine,

$$\left(X - D_n(s)\frac{\delta p}{p}\right)\cos(\alpha - \Delta\mu) + \left(X' - D_n'(s)\frac{\delta p}{p}\right)\sin(\alpha - \Delta\mu) = \frac{4\pi}{S}Q'\frac{\delta p}{p} \,. \tag{46}$$

To superimpose the extraction separatrices, the momentum dependence has to be removed from Eq. (46). This is true if,

Hardt condition:
$$D_n\cos(\alpha - \Delta\mu) + D_n'\sin(\alpha - \Delta\mu) = -\frac{4\pi}{S}Q' \,. \tag{47}$$

In practice, there is usually enough flexibility in D_n, D_n', and Q' to satisfy Eq. (47) with non-zero values. This corresponds to the Hardt condition being applied to the case of the momentum-driven extraction.

There is a second possibility of making $D_n = D_n' = Q' = 0$. Clearly zero chromaticity does not work for the momentum-driven extraction, but the amplitude-driven extraction can work with zero, or rather near-zero, chromaticity. The amplitude-driven extraction also uses a narrower beam in momentum, which makes the problem of aligning the separatrices less critical.

15 Numerical design

Although the above theory explains how slow extraction works and indicates the main configurations for the beams and equipment, this is not enough for designing a practical scheme. Most lattice programs will quickly reveal that separatrices are curved and the various parameters are not predicted with sufficient accuracy. It is therefore necessary to resort to a lattice program and to perform some trial and error calculations to set the spiral step precisely, to fine tune the Hardt condition and so on. Figure 14

shows the Hardt condition calculated for a momentum-driven extraction. Only the separatrices for the largest and the zero-amplitude ions are shown. It can be seen that these separatrices are curved and are not superimposed over their full length, but they have been made to cross at the ES using the Hardt condition theory and some trial-and-error refinements.

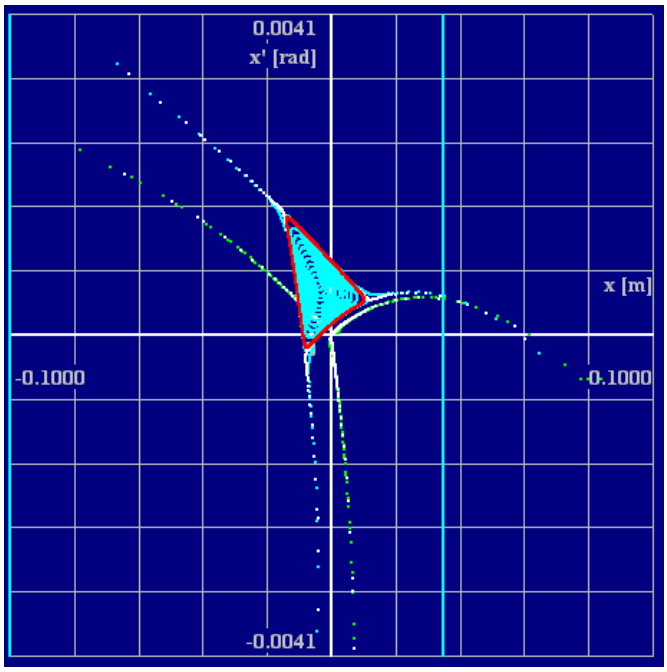

Fig. 14: The Hardt condition for a momentum-driven extraction (screen shot, WinAgile)

16 Getting to the MS

Another practical issue that depends on numerical calculation is the passage of the extracted beam segment between the ES and the MS. Depending on the lattice design, the extracted segment will stray beyond the edge of the machine aperture. The aperture between the ES and the MS is checked visually using a graphical method developed by C. Steinbach (CERN), see Fig. 15.

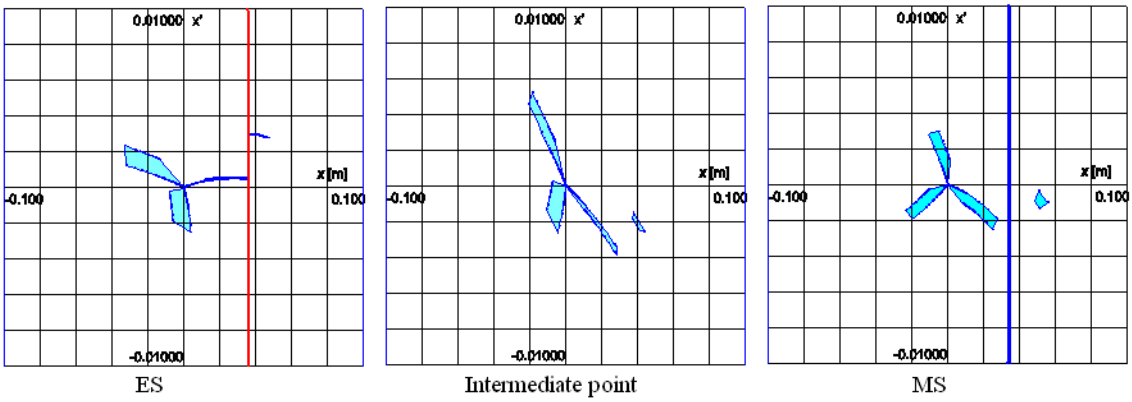

Fig. 15: Visual check of horizontal aperture from ES to MS (screen shots from WinAgile)

In Fig. 15, the phase-space areas between the maximum and the zero-amplitude separatrices are marked in light blue as well as the extracted beam segment. The efficiency of the method relies on the computer program being given all the aperture data for all the lattice positions between the ES and MS.

17 A 'strip' spill

It is now time to look more closely at how the ions cross the resonance and how this affects the spill. For mathematical convenience, the origin of the Hamiltonian is shifted to the upper fixed point and the extraction is considered via this fixed point, see Eq. (48) and Fig. 16.

$$\boldsymbol{H}_{\text{Shifted}} = \frac{S}{4}\left(4h^3 + 6hX^2 + 6\sqrt{3}hX\,X' + 3X\,X'^2 - X^3\right). \tag{48}$$

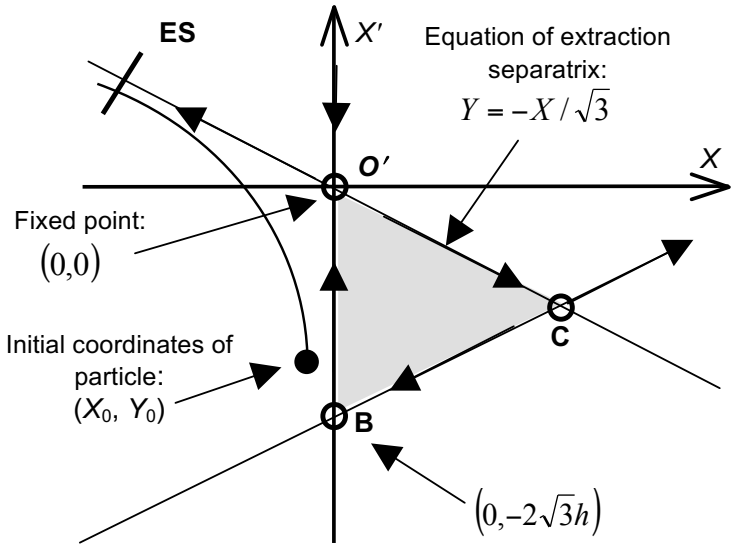

Fig. 16: Kobayashi Hamiltonian with shifted origin

The extraction process can be studied by considering what happens when the last stable triangle shrinks by a small step and a narrow strip of ions (coloured red) that were previously stable find themselves outside, in the unstable region, see Fig. 17. Only one of the three sides of the triangle is considered here. The black arrows show the general direction of movement of the ions. The grey arrows show the movement of the separatrices.

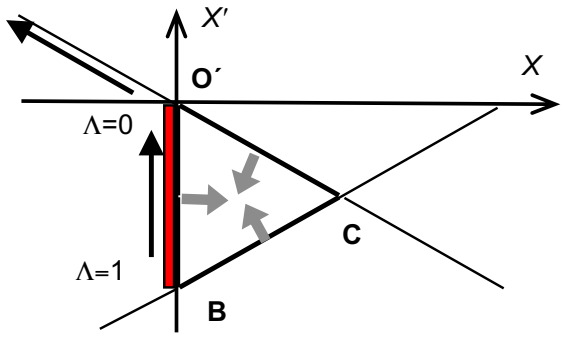

Fig. 17: Effect of shrinking the last stable triangle

In the translated frame of reference, the equations of motion become:

$$\frac{dX}{dt} = \frac{\partial \boldsymbol{H}}{\partial X'} = \frac{S}{4}\left(6\sqrt{3}hX + 6XX'\right). \tag{49}$$

$$\frac{dX'}{dt} = -\frac{\partial \boldsymbol{H}}{\partial X} = -\frac{S}{4}\left(12hX + 6\sqrt{3}hX' + 3X'^2 - 3X^2\right). \tag{50}$$

Extracted ions will follow paths of constant $\boldsymbol{H}$ close to the separatrices. The trajectories come directly from the initial conditions (X_0, X'_0) substituted into the Hamiltonian Eq. (48).

$$\frac{S}{4}(4h^3 + 6hX_0^2 + 6\sqrt{3}hX_0\,X_0' + 3X_0\,X_0'^2 - X_0^3) = \frac{S}{4}(4h^3 + 6hX^2 + 6\sqrt{3}hX\,X' + 3X\,X'^2 - X^3).$$

Close to the fixed point O′, ($|X|$, $|X'| << h$) and the third-order terms in X and X' can be neglected, so that

$$X' = \frac{X_0^2 + \sqrt{3}X_0X_0' - X^2}{\sqrt{3}X}. \tag{51}$$

Substituting Eq. (51) into the earlier expression for dX/dt in Eq. (49) gives the time profile. Note that time is dimensionless and is measured in steps of 3 turns.

$$\frac{\mathrm{d}X}{\mathrm{d}t} = \frac{S}{4}\left(6\sqrt{3}hX + \frac{6}{\sqrt{3}}X_0^2 + 6X_0X_0' - \frac{6}{\sqrt{3}}X^2\right). \tag{52}$$

Fortunately, Eq. (52) is a standard form that can be integrated.

$$\int \frac{\mathrm{d}x}{ax^2 + bx + c} = \frac{1}{\sqrt{b^2 - 4ac}} \ln\left|\frac{2ax + b - \sqrt{b^2 - 4ac}}{2ax + b + \sqrt{b^2 - 4ac}}\right|. \tag{53}$$

Within the strict assumptions made earlier ($|X|$, $|X'| << h$) , the result is only valid close to O′, but, since the particle approaches the separatrix asymptotically the third-order terms in the Hamiltonian cancel out, so they can also be neglected far from O′ along the outgoing separatrix and the integration can be extended right up to the ES.

The above analysis is used to find how long it takes for a particle to leave the machine. This is called the resonance ‘transit time’. The transit time is split into two parts:

- the time to travel from O′ to the ES; and
- the time to move along the side of the stable triangle from an arbitrary point towards O′.

Firstly, this is done under static conditions (while the stable triangle remains constant in size and position). In a second step these expressions must be modified to take into account the dynamic conditions of a shrinking stable triangle. The static result is shown in Eq. (54) and further results can be found in Refs. [9,10].

$$T_{\text{static}} \approx \frac{1}{\varepsilon\sqrt{3}} \ln\left| \underbrace{\frac{1}{(1-\Lambda_0)^2}}_{\substack{\text{Position on side of} \\ \text{triangle}}} \quad \underbrace{\left(\frac{n}{n+3}\right)}_{\substack{\text{Position of} \\ \text{electrostatic septum}}} \quad \underbrace{\frac{3}{\lambda_0}}_{\substack{\text{Distance} \\ \text{to triangle}}} \right|. \tag{54}$$

Firstly, Eq. (54) gives an estimate of the time needed for the first ions to arrive at the ES from the corner of the stable triangle.

Delay for first ions to arrive: $$t_0 \approx \frac{1}{\varepsilon\sqrt{3}} \,. \tag{55}$$

Secondly, it yields the same estimate for the length of time needed for all the ions along one side of the triangle to reach the corner. When these results are combined with estimates of the particle density along the sides of the triangle (the ions tend to concentrate at the corners and move speedily along the sides), the time profile of a strip spill is obtained, see Fig. 18. This profile shows a narrow spike of current after the delay given by Eq. (55) followed by a low flat spill of the same length as the initial delay. Typically, the initial delay is a few hundred time units (1 time unit being 3 turns).

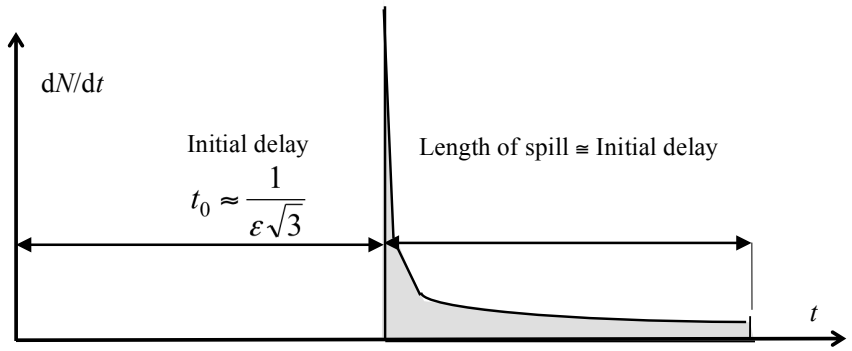

Fig. 18: Time profile of a strip spill

In the momentum-driven extraction (see Fig. 3), there is a range of momenta with stable triangles extending from zero to a maximum value (between points A and B). The smaller the area of the stable triangle, the smaller ε and the longer the transit time becomes. Combining all the strip spills leads to a so-called 'band' spill. Figure 19 shows an example.

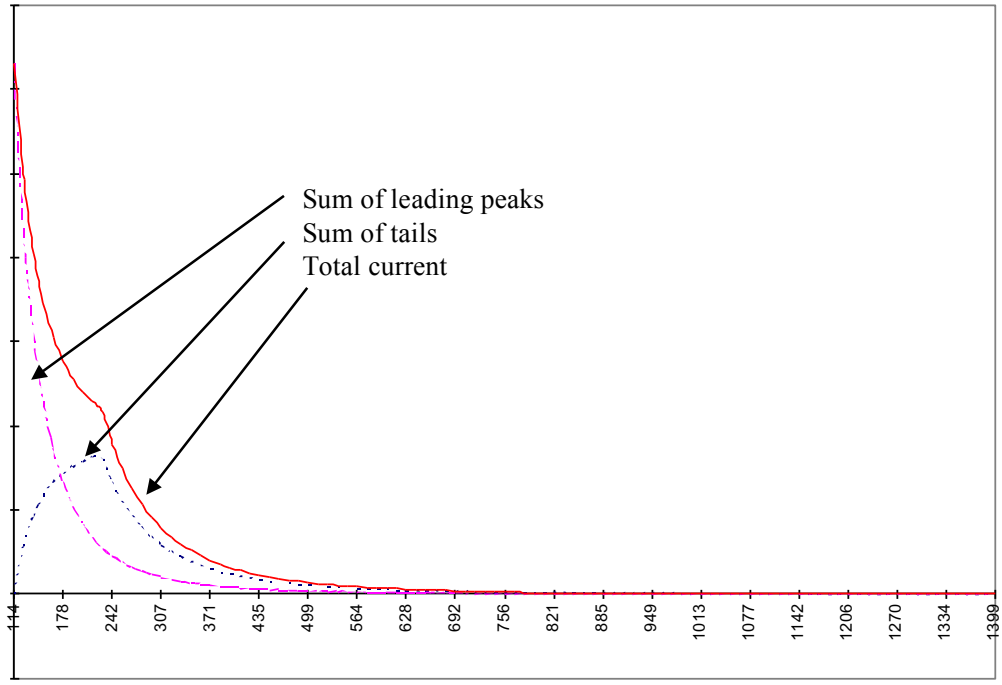

Fig. 19: Example of the time profile of a 'band' spill

18 Emittance of the extracted beam

The conservation of phase space (Liouville's Theorem) affords a simple and quick method for estimating and understanding the emittance of the extracted beam. Consider a coasting beam with a relatively large momentum spread. Assume that resonance is configured to give a significantly narrower momentum spread in the extracted beam. During the extraction, the separatrix acts like a knife shaving off the beam and its phase space. The transverse phase space and the longitudinal phase space ($\Delta p/p,\ t$) are jointly conserved as a phase-space volume. In the transverse plane, one can neglect the coupling to the vertical plane (in line with earlier approximations), so that the 'waiting' beam and the extracted beam have the same vertical emittance. The effect of the extraction can be seen by equating the phase-space volumes before and after the extraction and then looking at how the horizontal emittance in particular was affected. This is expressed quantitatively in Eq. (56) and illustrated schematically in Fig. 20.

$$E_{\mathrm{x,stack}}\left(\frac{\Delta p}{p}\right)_{\mathrm{stack}} T_{\mathrm{rev}} = E_{\mathrm{x,spill}}\left(\frac{\Delta p}{p}\right)_{\mathrm{spill}} T_{\mathrm{spill}}\ . \tag{56}$$

To give a quantitative impression, some orders of magnitude would be useful. Let the 'waiting' beam's horizontal emittance be $E_{\mathrm{x,beam}} = 10\pi \times 10^{-6}$ [m rad], $(\Delta p/p)_{\mathrm{beam}} = 0.005$, $T_{\mathrm{rev}} = 0.5 \times 10^{-6}$ [s], $(\delta p/p)_{\mathrm{spill}} = 0.001$, $T_{\mathrm{spill}} = 500\times 10^{-6}$ [s], so that $E_{\mathrm{x,spill}} = 50\pi \times 10^{-12}$ [m rad]. Thus, the long spill time compared to the short revolution time is balanced by the small transverse emittance of the spill compared to the much larger emittance of the 'waiting' beam. Under perfect conditions, this emittance would be seen as zero. However, the small horizontal emittance is often blown-up by ripple, noise, and imperfections in the optics. How big the horizontal emittance ends up is basically a question of power converter quality, optical precision, and various effects such as hysteresis and magnet time constants.

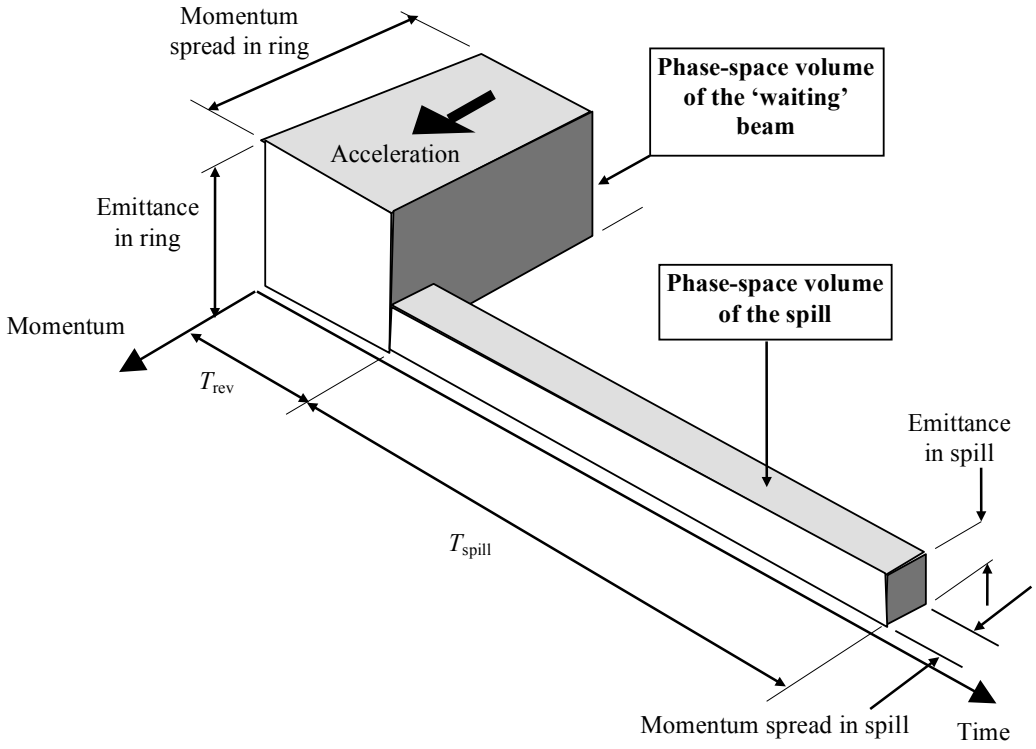

Fig. 20: Schematic view of the phase-space volume during extraction

19 A descriptive view of spill quality

19.1 Momentum-driven extraction

Momentum-driven, slow extraction can be likened to the shaving action on a wood-turning lathe, see Fig. 21. The projected width of the shaving is equivalent to the extracted $\delta p/p$, which is smaller than the width of the wood (i.e., the original beam $\Delta p/p$). The thickness of the shaving is related to the horizontal emittance of the extracted beam and the X-section of the wood is the original beam emittance. A typical extraction over one second in a machine with a revolution time of about one micro-second would require of the order of one million turns. This means that the shaving is extremely thin and the slightest vibration can cause the chisel to jump and chop the shaving, which gives rise to the legendary reputation of slow extractions for their sensitivity to ripple.

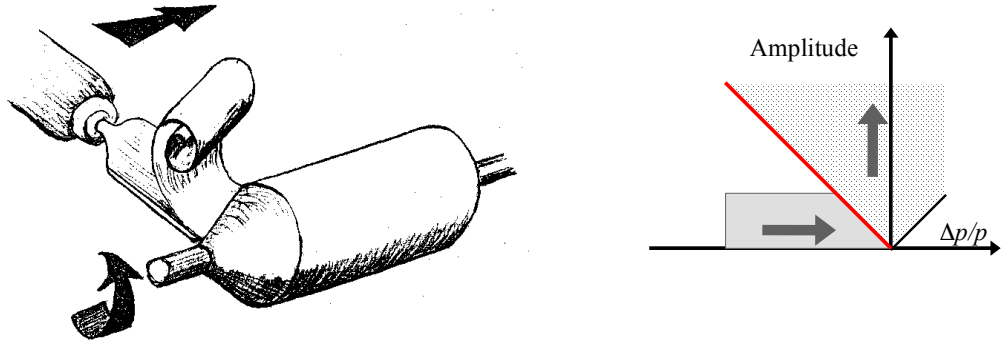

Fig. 21: Model of momentum-driven slow extraction

19.2 Amplitude-driven extraction

Amplitude-driven, slow extraction can also be likened to the shaving action on a wood-turning lathe, see Fig. 22. The width of the shaving is equal to the width of the wood and is equivalent to the $\Delta p/p$. The thickness of the shaving is the horizontal emittance of the extracted beam and the X-section of the wood is the original beam emittance. For ~1,000,000 turns, the shaving is extremely thin. As before, a typical extraction over one second in a machine with a revolution time of about one micro-second would require of the order of one million turns. This means that the shaving is extremely thin and the slightest vibration can cause the chisel to jump and chop the shaving.

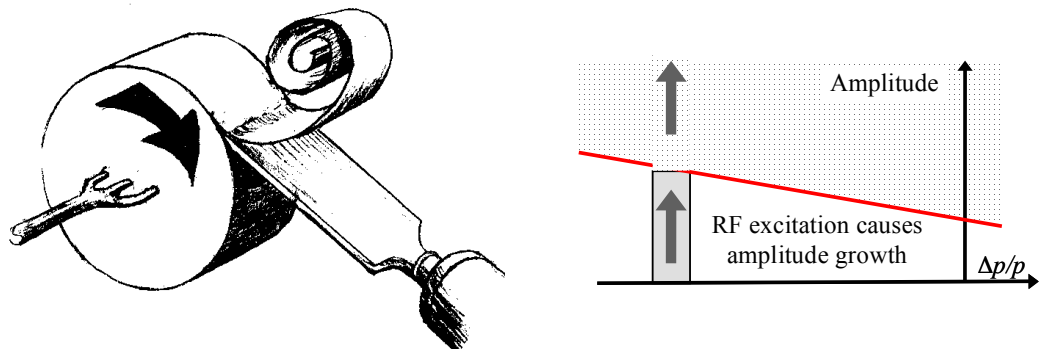

Fig. 22: Model of amplitude-driven slow extraction

20 Sensitivity to ripple

A simple analysis of the effects of ripple at low frequencies can be made by assuming that the particle flux that enters the resonance from the 'waiting' beam appears instantaneously in the observed spill. This is a fair approximation when the transit times in the resonance are small compared to the ripple frequency. Transit times depend upon the circumference of the machine, the strength of the resonance, the emittance, and so on. For a small medical synchrotron, the transit times typically vary from 100 turns up to 4,000 turns. There will always be a few particles that are quicker and few that are slower. For ease of computation, assume that most particles leave the machine within 2,000 turns. For a revolution time of 0.5 μs, this represents a generous delay of 1 ms. Thus, for 50 Hz, 100 Hz, and 300 Hz ripples (common in power converters), it is reasonable to say that extraction is instantaneous. With this simplified picture in mind, consider the schematic model shown below in Fig. 23. Whether the relative motion between the beam and the resonance is due to one partner, or both, is unimportant for the moment.

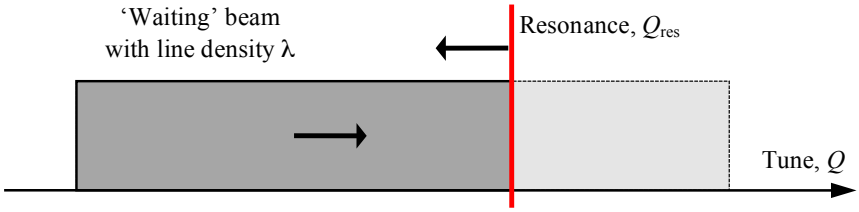

Fig. 23: Simple model for ripple

The relative motion between the beam and resonance will comprise a constant velocity, $(\mathrm{d}Q/\mathrm{d}t) = \dot{Q}_0$ plus a ripple term that may come from either the position of the beam via the main dipole field ripple or from the position of the resonance via the quadrupole ripple. Let the ripple have a sinusoidal form,

$$Q_r = \delta Q \sin(\omega t) \quad \text{so that} \quad \dot{Q}_r = \omega \delta Q \cos(\omega t) \,. \tag{57}$$

The flux of ions entering the resonance will be,

$$\phi = \frac{\mathrm{d}N}{\mathrm{d}t} = \lambda(\dot{Q}_0 + \dot{Q}_r) = \lambda(\dot{Q}_0 + \omega \delta Q \cos(\omega t)) \,, \tag{58}$$

where λ is the line density in the 'waiting' beam. By inspection, it is clear that while $\dot{Q}_0 > \omega\delta Q$ the spill will be continuous but modulated, whereas once $\dot{Q}_0 < \omega\delta Q$ the spill will be periodically 'chopped'. Thus, the critical ripple for a 'chopped' spill is given by

$$(\omega \delta Q)_{\text{critical}} = \dot{Q}_0 \,. \tag{59}$$

To give a quantitative impression, consider a typical small machine with T_{spill} = 1 s, Q_{res} = 1.666 and a tune spread necessary to consume the beam of ΔQ = 0.01. The average tune speed would be $\dot{Q}_0 = 0.01 s^{-1}$. The relationship of the tune ripple to the current ripple would be close to $\Delta Q / Q \approx \Delta I / I$. Some results are listed in Table 1. It is immediately apparent that just to stop the spill from being chopped requires exceeding tight specifications for the power supplies. Table 1 implies that extremely strict specifications for power supply ripple, transients and DAC steps are needed to prevent the chopping of the spill. For a project, it would be necessary to consider many more aspects before writing the power converter specifications. Some of these aspects will be considered in the next section.

Table 1: Conditions for 100% modulation of the spill at low frequencies ($dQ_0/dt = 0.01$, $Q_{res} = 1.666$)

Frequency [Hz]	$(\delta Q/Q_{res})_{critical} = \Delta I/I$
50	$2 \cdot 10^{-5}$
100	10^{-5}
300	$3.2 \cdot 10^{-6}$
1000	$9.6 \cdot 10^{-7}$

At higher frequencies, the spikes on the band spill (see Fig. 19) still appear as individual spikes, but the long tails overlap creating a uniform base spill containing about half of the ions topped by the narrow spikes. At much higher frequencies, the spikes start to overlap.

21 Handling ripple

21.1 Power converters

Switch-mode power converters have an advantage over the more conventional units, especially if switch-mode frequency can be placed above 20 kHz. Care must also be taken to ensure there is always a sufficient number of DAC steps in the current range to be ramped.

21.2 Eddy current smoothing

Normally, eddying currents are avoided in accelerators; to reduce field distortion and resistive losses during ramping. However, during a slow extraction, very stable conditions in the 1,000 Hz region are required for the main lattice elements and for the betatron core. Adjusting the lamination thickness of the main lattice magnets can be of help. This is of course a compromise—some resistive losses and distortion during ramping for some field smoothing on the extraction flat top.

21.3 Intrinsic smoothing

Referring back to the ‘strip’ spill in Fig. 18 and the ‘band’ spill in Fig. 19, the former is a close approximation of what happens in a RF, amplitude-driven extraction while the latter corresponds to what occurs in the momentum-driven extraction with a betatron core. Clearly, there is some advantage in the momentum-driven extraction with the band spill, because the narrow peaks are spread out. This is known as ‘intrinsic smoothing’.

21.4 Front-end acceleration

Figure 24 gives a pictorial view of a momentum-driven extraction. In the analogy, the ‘beam ions’ are moved slowly into the resonance by a plunger that pushes the ions across a vibrating platform. In the case shown, the vibrations dominate the slow acceleration and they wobble on the edge of the platform shaken by the vibrations (ripple) until they fall off the platform (and into the resonance) in an uncontrolled way.

The spill can be desensitized to the ripple by increasing the velocity of the ‘beam ions’ as they reach the edge of the platform, so that their velocity is greater than the perturbation caused by the ripple. Figure 25, shows the same analogy as Fig. 24, except that the ‘beam ions’ now sprint forward just before the edge of the platform, so that the vibrations becomes less influential. This is called ‘front-end’ acceleration and can be done by ‘empty-bucket’ channelling (see next section) or by RF noise.

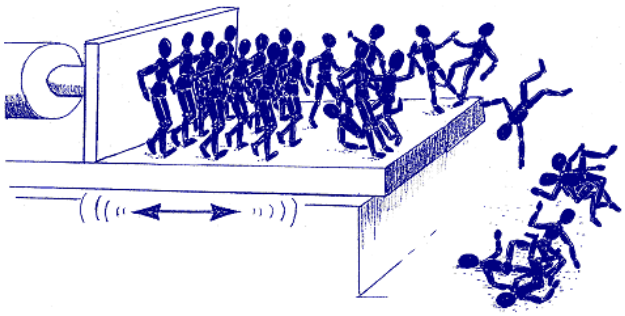

Fig. 24: No addition 'front-end' acceleration

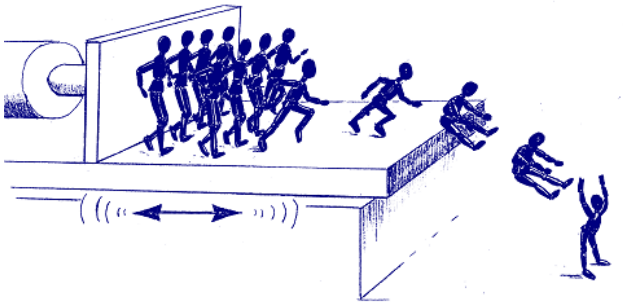

Fig. 25: 'Front-end' acceleration stabilizes ions as they pass into resonance

21.5 Empty-bucket channelling

The 'front-end' acceleration mentioned in the previous section can be achieved by 'empty-bucket' channelling [11, 12]. The betatron core slowly accelerates the beam into the resonance (upwards in Fig. 26). The empty RF buckets are nearly stationary. If they were to be filled with beam, they would accelerate their beam in the opposite sense to the betatron core at the same speed. When the slowly moving beam meets the empty buckets, it has to stream round the buckets through a narrow phase-space gap at a much higher speed to maintain the flow. This is similar to the rapid movement of water between the piers of a bridge.

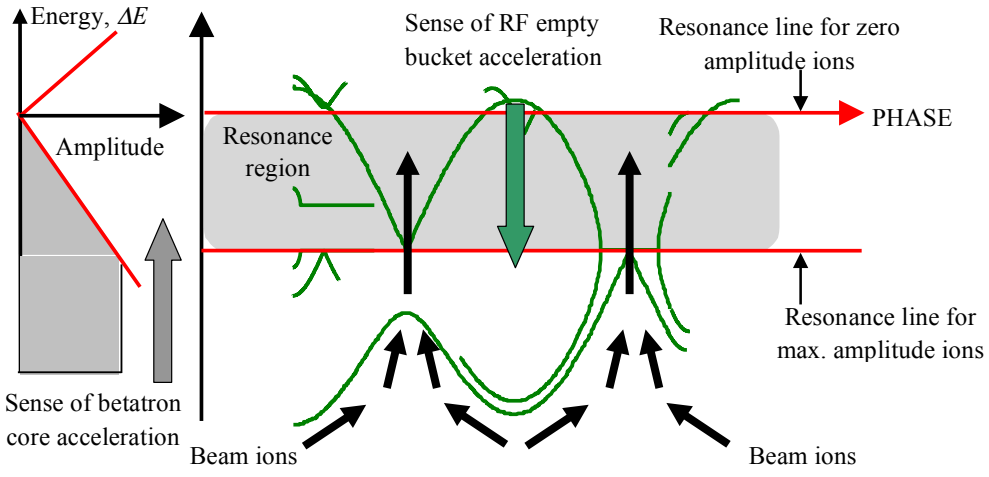

Fig. 26: Empty-bucket channelling

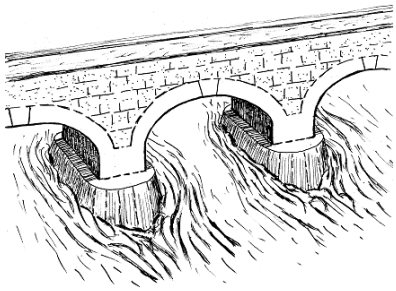

Fig. 27: The bridge analogy to empty-bucket channelling

22 Small horizontal beam size

The mono-energetic extracted beam segment (see Figs. 5 and 9) is typically 10 mm long and 0.1 mrad wide and is known as the 'bar of charge'. These dimensions are very approximate and depend on the power converter ripple and the optics errors as mentioned in section 19. For the momentum-driven extraction there is a continuum of segments of different momenta. If the Hardt condition is applied these segments are all superimposed and the 'bar of charge' is again 10 mm by 0.1 mm.

Those designing an extraction should note that the detailed optics at the entrance to the ES are rather complicated. At this position, there is one set of Twiss parameters that belongs to the ring. In the vertical plane these parameters are handed on to the extraction line, BUT NOT in the horizontal plane. In the horizontal plane, careful tracking will reveal that the segments of different momenta have different lengths and have their low momentum sides aligned. First one should choose a central segment to define the momentum and position of the central orbit for the extracted beam. Next the relative positions of the segments with respect to this central orbit define the dispersion vector for the entry to the extraction line. Finally, the rectangular shape of the segments is not convenient for fitting to a betatron ellipse. If one tries to fit inscribed or circumscribed ellipses to all the segments a rather complicated situation is created with potentially exotic optics. One solution is to forget ellipses and to treat the 'bar of charge' as the diameter of an unfilled ellipse, see Fig. 28.

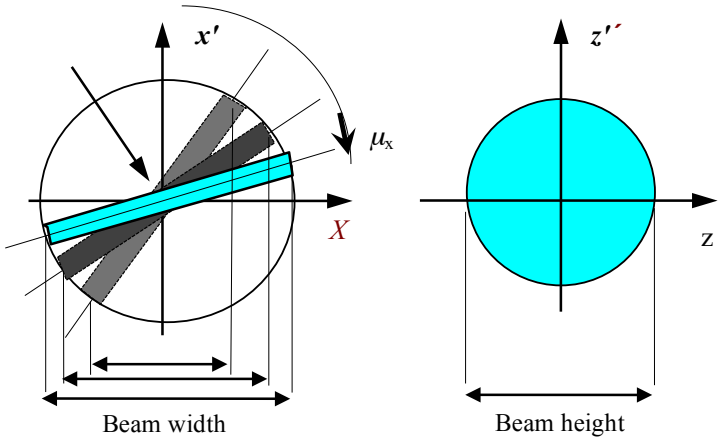

Fig. 28: Controlling beam width and height

Using the concept of an unfilled ellipse creates well-behaved optics that are relatively insensitive to changes in the width of the 'bar of charge' that will vary for example because ripple is more serious at low extraction energies than at top energy. For the unfilled ellipse, the width of the beam is defined by the projection of the 'bar of charge' on the *x*-axis. If a phase shifter is introduced in the line, then the

'bar' can be rotated. This rotation changes the beam width at the patient from a minimum value set by the width of the 'bar' up to a maximum value set by the length of the segment (see Fig. 28). The beam height is the projection of the Gaussian beam distribution in the vertical plane on the z-axis and can be changed by a 'betatron stepper'.

23 Scanning

As explained above, the extracted beam spot distributions are near-uniform over a narrow rectangle in the horizontal phase space and near-Gaussian in the vertical phase space. For voxel scanning, overlapping Gaussian spots give a smooth deposition of beam, whereas overlapping rectangles give 'hot/cold' ridges. The procedure is to scan with the Gaussian distribution aligned to the 'slow' scanning direction (from row to row), since errors are more likely to build up over time between rows and then to scan in the fast direction (along a row) taking mini-steps (say 1/5th of the voxel width). Since the beam spot is not perfectly rectangular, but has some rounding at the edges, this scheme works well.

24 Rotational matching to a gantry

In the extraction line of a medical facility, a rather special situation is met in which a fixed transfer line must be matched to a section of line called the gantry that has to be able to rotate through a full $0 \rightarrow 2\pi$ without affecting the beam spot at the patient, see Fig. 29. In cyclotron-based facilities, the problem is solved by making the beam distribution rotationally symmetric at the interface between the fixed and rotating lines. A rotationally symmetric beam requires equal emittances, equal lattice parameters, equal particle distributions and zero dispersion. Unfortunately, the slow-extracted beam from a synchrotron, as described in this lecture, is far from fulfilling these requirements (rectangular/Gaussian). A lot can be written on this topic about various restricted solutions and similar problems, but the only truly rotational solution that also includes the dispersion vector is the 'rotator' method attributed to Lee Teng [13]. This solution is extremely elegant and can be approached from a purely mathematical viewpoint.

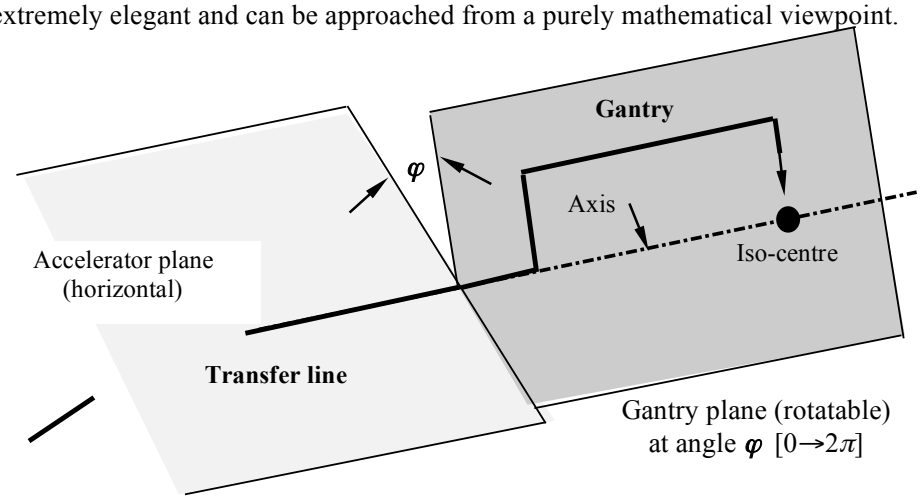

Fig. 29: Schematic view of an iso-centric gantry and transfer line

Consider a section of bending-free transfer line with a betatron phase advance of 2π in the x-plane and π in the z-plane. This section of line will be called a 'rotator'. According to the phase advances, the transfer matrix for the rotator will be;

$$M_{\text{rotator}} = \begin{pmatrix} 1 & 0 & 0 & 0 \\ 0 & 1 & 0 & 0 \\ 0 & 0 & -1 & 0 \\ 0 & 0 & 0 & -1 \end{pmatrix}. \tag{60}$$

Let this line be rotated by an angle ν with respect to the fixed transfer line and let ν be just half of the rotation angle of the gantry, 2ν. A schematic view is shown in Fig. 30.

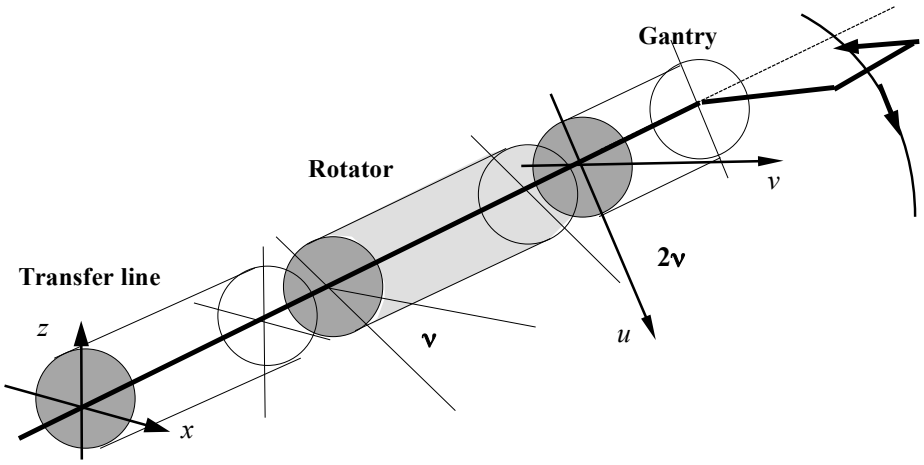

Fig. 30: Equipment layout for the rotator method

The transfer matrix from the exit of the fixed beam line to the interface point at the entry to the gantry is found by multiplying the rotation matrix for the angle ν, the rotator and a second rotation matrix also for the angle ν.

$$\begin{pmatrix} \cos\nu & 0 & \sin\nu & 0 \\ 0 & \cos\nu & 0 & \sin\nu \\ -\sin\nu & 0 & \cos\nu & 0 \\ 0 & -\sin\nu & 0 & \cos\nu \end{pmatrix} \begin{pmatrix} 1 & 0 & 0 & 0 \\ 0 & 1 & 0 & 0 \\ 0 & 0 & -1 & 0 \\ 0 & 0 & 0 & -1 \end{pmatrix} \begin{pmatrix} \cos\nu & 0 & \sin\nu & 0 \\ 0 & \cos\nu & 0 & \sin\nu \\ -\sin\nu & 0 & \cos\nu & 0 \\ 0 & -\sin\nu & 0 & \cos\nu \end{pmatrix}$$

$$= \begin{pmatrix} \cos^2\nu + \sin^2\nu & 0 & \sin\nu\cos\nu - \cos\nu\sin\nu & 0 \\ 0 & \cos^2\nu + \sin^2\nu & 0 & \sin\nu\cos\nu - \cos\nu\sin\nu \\ -\sin\nu\cos\nu + \cos\nu\sin\nu & 0 & -\cos^2\nu - \sin^2\nu & 0 \\ 0 & -\sin\nu\cos\nu + \cos\nu\sin\nu & 0 & -\cos^2\nu - \sin^2\nu \end{pmatrix}.$$

After a simple reduction of the terms, the final overall transfer matrix maps the incoming normal modes directly to those of the gantry without any cross-coupling and independently of the rotation angle.

Rotator:

$$\begin{pmatrix} u \\ u' \\ v \\ v' \end{pmatrix}_{\text{Gantry}} = \begin{pmatrix} 1 & 0 & 0 & 0 \\ 0 & 1 & 0 & 0 \\ 0 & 0 & -1 & 0 \\ 0 & 0 & 0 & -1 \end{pmatrix} \begin{pmatrix} x \\ x' \\ z \\ z' \end{pmatrix}_{\text{Input}}. \tag{61}$$

Since a dispersion vector in a bending-free region behaves as a betatron oscillation to first order, the rotator will automatically match the dispersion vector (*D, D'*) into the gantry at the same time as it matches the normal modes. There are no fundamental limitations on the beam distributions or any of the Twiss or dispersion functions. The matching is entirely independent of the gantry rotation angle. This is important for the slow extraction from a synchrotron because the beam shape (rectangular/Gaussian) will always have the same orientation in the gantry nozzle whatever the gantry angle. Note, however, that the beam is coupled inside the rotator.

The rotator as presented is a purely mathematical solution. For example, four FODO cells with $\pi/2$ phase advance horizontally and $\pi/4$ phase advance vertically would satisfy the conditions, but would not be a practical solution because the beam sizes inside the rotator would be impractically large. To achieve well-behaved beam sizes within the rotator the trick is to make the Twiss alpha functions zero in both planes at the entry and exit. Figure 31 shows a well-behaved triple-triplet rotator design.

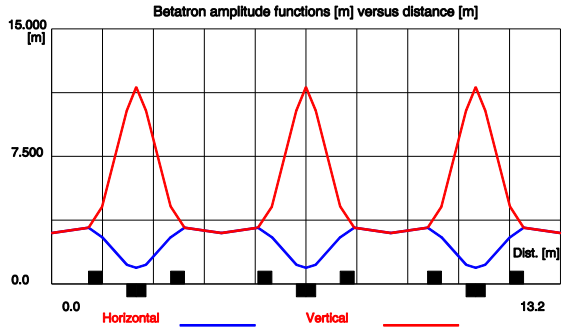

Fig. 31: Triple-triplet rotator ($\beta_x = \beta_z = 3$ m, $\alpha_x = \alpha_z = 0$, $L = 13.2$ m, $k_F = -k_D$)

25 Beam cut-off

Cutting the beam off is a security problem in medical machines. Amplitude-driven, slow extraction has the advantage that the RF excitation driving the amplitude growth can be switched off quickly and since the extraction works only with large amplitude ions the transit time in the resonance is short making the overall switching time a few tens of microseconds, whereas, momentum-driven, slow extraction is a little slower to respond. Not only is the betatron core slower than RF, there are a few small amplitude ions trapped in the resonance that can take a millisecond or two to transit. In both cases, the switch-off can be made to satisfy treatment safety, but to satisfy the wider needs of security there has to be an independent cut-off mechanism that is less reliant on software links.

The usual solution is to place four identical ferrite dipoles powered in series in a single straight section in the transfer line to excite a closed-orbit bump that holds the beam clear of a dump block, see Fig. 32. By switching off the dipoles, or in the event of a power failure, the beam drops onto the dump. The switching time can be less than 200 microseconds.

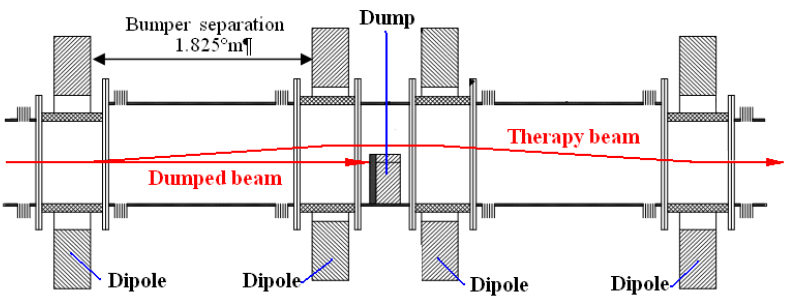

Fig. 32: Beam chopper

References

[1] The possibility of resonant extraction from the CPS, CERN-AR-Int-GS-61-5.

[2] C.L. Hammer and L.J. Laslett, *Rev. Sci. Instr.* **32** (1962) 144−149, https://doi.org/10.1063/1.1717299.

[3] Y. Kobayashi and H. Takahashi, Improvement of the emittance in the resonant ejection, Proc. VIth Int. Conf. on High Energy Accelerators, Cambridge, Massachusetts, 1967, pp. 347−51.

[4] M.Q. Barton, Beam extraction from synchrotrons, Proc. VIIIth Int. Conf. on High Energy Accelerators, CERN, Geneva, 1971, pp. 85−8.

[5] G. Guignard, A general treatment of resonances in accelerators, CERN 78-11 (CERN, Geneva, 1978), https://doi.org/10.5170/CERN-1978-011.

[6] K. Hiramoto and M. Nishi, *Nucl. Instr. Meth. in Phys. Res.* **A3320** (1992), p. 154, https://doi.org/10.1016/0168-9002(92)90023-W.

[7] PIMMS, Proton-ion medical machine study, Study Leader and Editor P.J. Bryant, CERN 2000-006, (CERN, Geneva, 2000), https://doi.org/10.5170/CERN-2000-006.

[8] Ultraslow extraction out of LEAR (transverse aspects*),* CERN Internal Note PS/DL/LEAR Note 81-6, (1981).

[9] M. Pullia, Transit time for third order resonance extraction, CERN/PS 96-36 (DI).

[10] M. Pullia, Time profile of the slowly extracted beam, CERN/PS 97-50 (DI).

[11] R. Cappi and C. Steinbach, Low Frequency Duty Factor Improvement for the CERN PS Slow Extraction Using RF Phase Displacement Techniques, 1981 Particle Accelerator Conference, Washington, 11−13 March 1981.

[12] RF Empty Bucket Channelling Combined With a Betatron Core to Improve Slow Extraction in Medical Synchrotrons, CERN/PS 97-68 (DI).

[13] L.C. Teng, Private communication, Laboratory notebook (Jan. 1970) and Int. Rep. LL-134 (Oct. 1986).